 

DOI: 10.1070/QEL16038

# Periodic colour-centre structure formed under filamentation of mid-IR femtosecond laser radiation in a LiF crystal

A.V. Kuznetsov, V.O. Kompanets, A.E. Dormidonov, S.V. Chekalin, S.A. Shlenov, V.P. Kandidov

*Abstract.* **A colour-centre structure formed in a LiF crystal under filamentation of a femtosecond mid-IR laser pulse with a power slightly exceeding the critical power for self-focusing has been experimentally and theoretically investigated. Strictly periodic oscillations have been detected for the first time for the density of the colour centres induced in an isotropic LiF crystal under filamentation of a laser beam with a wavelength tuned in the range from 2600 to 3350 nm. The structure period is found to be about 30 μm. With an increase in the laser radiation wavelength, the period of the oscillations decreases and their amplitude increases. The maximum colour centre density, observed under filamentation of a 3100-nm beam, is related to the increased contribution of the direct generation of colour centres as a result of the absorption of an integer number of photons by the exciton band. It is numerically shown that the formation of a periodic colour-centre structure in LiF is due to the periodic change in the light field amplitude in the light bullet (1.5 optical periods long) formed under filamentation.**

***Keywords:*** *filamentation, femtosecond pulses, anomalous dispersion, light bullets, colour centres, LiF.*

## 1. Introduction

The development of high-power laser systems made it possible to localise light fields without any waveguide systems; this localisation manifests itself in the form of extended filaments of high energy density [1–4]. Russian researchers played an important role in all stages of studying the phenomena of laser beam self-focusing and filamentation [5].

The concentration of laser energy in an extended filament, generation of supercontinuum and THz radiation, formation of plasma channels, and other effects accompanying femtosecond filamentation immediately attracted attention of researchers in view of the practical importance of these phenomena. The effects occurring under femtosecond filamentation expand the range of application of new laser technologies in ecology, biophysics, atmospheric optics, microoptics, and other fields. Examples are as follows: energy transfer by distances of several kilometres to form optical breakdown plasma and luminescence signal in distant monitoring of contaminations, broadband laser environmental sensing [6, 7], use of plasma channels for directed microwave radiation transfer [8] and design of microoptics elements [9, 10].

Much attention is paid to the filamentation regime, in which simultaneous laser beam self-focusing and pulse self-compression lead to the formation of so-called light bullets (LBs) [11]. A necessary condition for implementing this regime is the existence of anomalous group-velocity dispersion (GVD), which, in the case of self-phase modulation of the light field in a medium with Kerr nonlinearity, may cause formation of an LB (wave packet compressed in space and time). Under conditions of anomalous GVD, the phase-modulated light field is 'contracted' to the centre of the pulse from its leading and trailing edges [12]. The pulse compression in time and in space as a result of its compression under anomalous GVD and self-focusing due to the Kerr nonlinearity, self-steepening of the leading and trailing edges, and defocusing of the pulse tail in the induced plasma form an LB in the filament [13–15]. As was shown in [13–15], the peak intensity in the bullet reaches $5 \times 10^{13}$ W cm$^{-2}$, and its diameter (in fused silica) is 20 μm. The shape of the LB field envelope differs strongly from Gaussian. At the centre wavelength ($\lambda_0$ = 1800 nm), the LB width amounts to 13.5 fs, i.e., about two light field oscillation periods. The evolution of the LB spatial and temporal structure at $\lambda_0$ = 1800 nm in sapphire was investigated by Majus et al. [16]. They proposed a scenario, according to which an LB, like a Bessel beam, consists of a high-intensity core (containing more than 25% of the total energy) and a low-intensity periphery.

The question about the behaviour (quasi-steady-state [17] or recurrence [13–15]) of LB propagation in a medium is still debated. A long luminous channel of scattered supercontinuum radiation in the visible range, formed under filamentation at $\lambda_0$ = 1900 nm in fused silica, was interpreted in [17] as a long-lived quasi-soliton, which is retained at a distance of several centimetres. The possibility of forming a sequence of LBs during filamentation under anomalous GVD conditions was numerically investigated in [18]. According to [19], the formation of subsequent LBs in a sequence may be violated both at low GVD (due to the insufficient compression of the phase-modulated field) and at high GVD (because of the significant broadening of the pulse during its propagation before the filament formation). The generation of a sequence of short-lived LBs was confirmed both experimentally (by autocorrelation measurements) and theoretically in [14, 15, 20]. It was established in [21, 22] that the formation of each LB in a sequence is accompanied by 'ejection' of an equal amount of

**A.V. Kuznetsov** Institute of Laser Physics (Irkutsk Branch), Siberian Branch, Russian Academy of Sciences, ul. Lermontova 130a, 664033 Irkutsk, Russia; e-mail: a.v.kuznetsov@bk.ru;
**V.O. Kompanets, S.V. Chekalin** Institute of Spectroscopy, Russian Academy of Sciences, ul. Fizicheskaya 5, Troitsk, 108840 Moscow, Russia; e-mail: chekalin@isan.troitsk.ru;
**A.E. Dormidonov, S.A. Shlenov, V.P. Kandidov** Department of Physics and International Laser Centre, M.V. Lomonosov Moscow State University, Vorob'evy Gory, 119991 Moscow, Russia

Received 8 February 2016
*Kvantovaya Elektronika* **46** (4) 379–386 (2016)
Translated by Yu.P. Sin'kov

supercontinuum energy in the visible range. The LB energy is transformed into the supercontinuum energy in the entire spectral range; this process is the main channel of LB degradation. It was found that LB is a stable self-organizing object, which is independent of the input parameters, such as the spatial and temporal shape of the pulse and its phase. An important (and still poorly studied) problem of filamentation is related to the influence of the absolute phase [23] in the case of propagation of LBs containing few light-wave periods through a transparent medium [24].

In this paper, we report the results of experimental and theoretical study of a periodic colour-centre (CC) structure induced in an isotropic LiF crystal by a single LB, formed in the single-filamentation mode by a femtosecond mid-IR (2600–3350 nm) laser pulse with a power slightly exceeding the critical power for self-focusing. Based on numerical simulation data, it is shown that the observed CC structure is formed due to the periodic oscillations of the maximum light field amplitude in an LB with a width of 1.5 optical oscillations during its propagation in a dispersive medium.

## 2. Experimental technique

The LB dynamics was studied using the method proposed in [25], which is based on the generation of stable luminescence CCs in a LiF crystal under laser irradiation. The LiF photosensitivity is sufficiently high to record LB tracks under filamentation of single femtosecond laser pulses. The spatial luminescence intensity distribution for the recorded CCs reproduces the density of laser-induced electronic excitations in a filament. The CC luminescence intensity distribution is analysed by optical microscopy, with illumination at the absorption wavelength for these CCs.

Alkali metal fluorides are promising materials for studying the filamentation in the mid-IR range, because they have anomalous GVD in this spectral region (a necessary condition for the LB formation). The spectral transparency windows of fluorides overlap the UV and IR ranges; this is an important condition for supercontinuum generation. The generation of a broadband supercontinuum was investigated under filamentation of radiation with $\lambda_0 = 2000$ nm in $CaF_2$ [26] and $\lambda_0 = 800$, 1380, and 2200 nm (falling in the ranges of normal, zero and anomalous GVD) in $BaF_2$ and $CaF_2$ [27]. Alisauskas et al. [28], who investigated the filamentation of radiation at $\lambda_0 = 3900$ nm in $CaF_2$ and some other crystals, observed radiation in the form of a supercontinuum in the visible range, without spectral broadening in the vicinity of the fundamental frequency; they explained this effect by the CC luminescence. A study of the filamentation of mid-IR radiation in $BaF_2$ and $CaF_2$ [29] revealed an isolated band in the visible spectral range; the blue shift of this band increases and its width decreases from 50–70 nm to 14 nm with an increase in the radiation wavelength from 3000 to 3800 nm.

The choice of LiF as a material for studying the LB dynamics is determined by the highest intensity of the CC luminescence in it in comparison with other alkali halide crystals, due to which one can observe a laser-induced modification of material under single-pulse filamentation. In addition, CCs in LiF have high thermal and optical stability at room temperature; hence, CC structures can be investigated by different methods after recording them. Finally, LiF is less hygroscopic and more convenient for mechanical treatment in comparison with many other alkali halide crystals.

The CCs in LiF that are most appropriate for investigating filamentation are $F_2$ and $F_3^+$, which emit in the visible range. These centres are, respectively, a dyad and a triad of anionic vacancies in neighbouring lattice sites, with a captured electron pair. The luminescence bands of these centres are peaking near $\lambda = 650$ and 550 nm, respectively [30]. Centres of both types are excited by blue light. It is known [31] that an irradiation of LiF by a femtosecond laser beam with $\lambda_0 = 800$ nm leads to preferred generation of $F_3^+$ centres, whereas the generation of $F_2$ centres is dominant upon X-ray excitation.

The colouring of a material can be explained by both nonlinear photoexcitation of its electron subsystem with the formation of excitons and electron–hole pairs via avalanche, tunnel and multiphoton ionisation and through direct excitation of excitons [32–34]. The decay of excitons and electron--hole pairs leads to the formation of the simplest F centres, which are single anionic vacancies with a captured electron [35]. The characteristic time of this process in alkali halide crystals is several picoseconds [36]; therefore, it occurs after the passage of a femtosecond laser pulse. An aggregation of different numbers of anionic vacancies and F centres gives rise to luminescence aggregate CCs, including $F_2$ and $F_3^+$, which emit light under blue illumination.

## 3. Experimental results

Experiments were performed using a laser radiation source based on a femtosecond Tsunami generator (Ti:sapphire laser) with a cw solid-state Millenia Vs pump laser, regenerative Spitfire Pro amplifier with a pumping solid-state Empower 30 laser, and a tunable parametric TOPAS amplifier. The pulse FWHM was 100 fs, the spectral half-width was 200–250 nm and the pulse repetition rate was varied from 1 kHz to the minimum (single-pulse regime). The pulse energy (measured by a Fieldmax sensor with a PS-10 detector) was about 10 μJ. Laser pulses were focused by thin $CaF_2$ lenses with a focal length $F = 15$ or 10 cm in a 40-mm-long LiF sample at a distance of several millimetres from its input face. When recording CCs in the single-pulse exposure regime, the sample was displaced in the direction perpendicular to the laser beam after each pulse. CCs were recorded in LiF samples by beams with three wavelengths: 2600, 3100 and 3350 nm; both lenses were alternately used. To implement the single-filamentation regime with variation in wavelength, the energy of pulses was changed so as to make their peak power somewhat exceed the critical power for self-focusing. The pulsed radiation energy at $\lambda_0 = 2600$, 3100 and 3350 nm was, respectively, 10.1, 11.5 and 13.5 μJ. In addition, the sample was irradiated at $\lambda_0 = 3100$ nm with a change in energy from 9 to 15.6 μJ.

To perform high-quality analysis of recorded CC structures, we used an Euromex Oxion $5^{\times}$ microscope with illumination by a cw laser beam at $\lambda = 450$ nm; the luminescence signal was detected by a Nikon D800 digital camera. The scattered excitation light was cut off by an auxiliary yellow-green light filter. Photographs of a series of luminescence structures induced in LiF at $\lambda_0 = 3100$ nm are shown in Fig. 1. An irradiation of an immobile crystal with a pulse repetition rate of 100 Hz led to the formation of intense luminescence tracks in the sample, which can be seen in Fig. 1 as the brightest horizontal lines of large thickness and extension. When the sample was displaced, luminescence CC structures induced by single pulses were observed between its stop points; they

can be seen in Fig. 1 as thin horizontal lines with a periodically varied brightness. The random longitudinal displacement of the induced structures along the filament is caused by laser pulse energy fluctuations. The characteristic length of the structures is about 1 mm, and their transverse size is 2–3 μm.

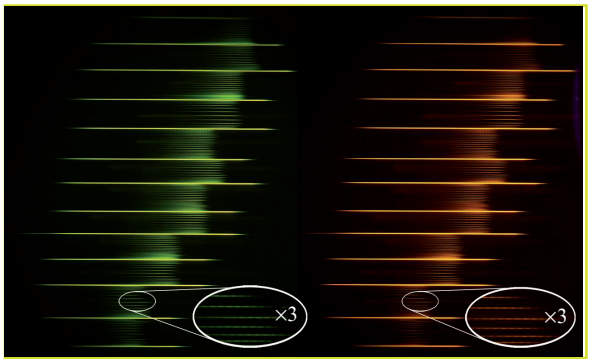


**Figure 1.** (Colour online) Photographs of the same series of luminescence structures induced in LiF by a pulsed laser beam with $\lambda_0$ = 3100 nm and different energies (from 9 μJ in the lower fragment of the image to 15.6 μJ in the upper fragment). The bright lines dividing fragments correspond to recording CCs under multipulse exposure, and the thin lines in the fragments were obtained with a single-pulse exposure. The luminescence signal was excited by a cw laser at $\lambda$ = 450 nm (the excitation power for the right column exceeds that for the left column). Image fragments magnified thrice are shown in the bottom; they exhibit periodic changes in the luminescence brightness for the structures induced by single pulses.

The detection of two CC luminescence colours (Fig. 1) confirms the presence of $F_2$ and $F_3^+$ centres in the recorded structures. Radiation with $\lambda$ = 450 nm excites simultaneously $F_2$ and $F_3^+$ centres. At low excitation intensities, the luminescence of $F_3^+$ CCs with a maximum at $\lambda \approx$ 550 nm is dominant, whereas the contribution of the luminescence of $F_2$ centres with a maximum at $\lambda \approx$ 650 nm to the total luminescence signal is small. At high excitation intensities, an effect related to the transition of $F_3^+$ CCs to the metastable nonradiative state with a lifetime of several seconds manifests itself. This circumstance leads to a decrease in the observed $F_3^+$ luminescence intensity in comparison with the luminescence of $F_2$ CCs, which do not pass to the nonradiative state, and the luminescence of the latter becomes dominant. The lines in the right column in Fig. 1 were obtained at $\lambda$ = 450 nm with a higher excitation intensity than the lines in the left column, which resulted in different luminescence colours of laser-induced structures: orange and green colours on the right and on the left, respectively.

## 4. Processing of experimental results

### 4.1. Period of CC density oscillations

To study in detail the periodic changes in the CC structures induced by single pulses in LiF, we used an Olympus IX 71 microscope with a 10× objective and an Olympus E520 digital camera with a yellow-green filter, which cuts off scattered excitation radiation at $\lambda$ = 450 nm. When recording series of luminescence structures by the camera, the exposure time was chosen sufficiently short to exclude saturation of the photosensitive camera array by the luminescence signal. The period of CC density oscillations in the induced structures was found using digital processing of the photographs, in which a two-dimensional coloured image was transformed into a monochromatic one by summing the red and green components of pixels in digitised photographs (the blue component was rejected as containing no useful signal), after which the values for the pixels in the cross section perpendicular to the structure axis were summed. The background (assumed to be equal to the signal for the pixels located beyond the structure image) was subtracted from the total luminescence signal. The thus obtained luminescence signal profiles for individual structures induced by femtosecond pulses are presented in Fig. 2 (solid curves). The initial image of the corresponding structure is located under each profile. The luminescence signal is proportional to the linear CC density in the structures. The longitudinal luminescence intensity profiles exhibit CC density oscillations against the background of regular slow changes, obtained by smoothing the corresponding structural profiles (dashed curves). Note that the amplitude of CC density oscillations increases significantly with an increase in wavelength from 2600 to 3350 nm. The distance on which CCs are generated is ~1 mm, which corresponds to the interval of existence of filamentation-induced LB [21, 22].

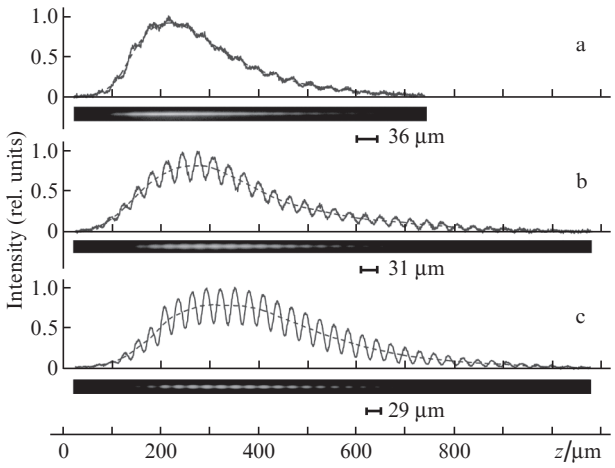


**Figure 2.** Longitudinal luminescence intensity profiles (solid curves) for the CC structures induced in LiF by single 100-fs pulses, regular slow changes in intensity (dashed curves) and the corresponding images of the initial structure (bottom) under the following conditions: (a) radiation wavelength $\lambda_0$ = 2600 nm and pulse energy $W$ = 10.1 μJ, (b) $\lambda_0$ = 3100 nm and $W$ = 11.5 μJ and (c) $\lambda_0$ = 3350 nm and $W$ = 13.5 μJ. The laser beam propagates from the left to the right. The lens focal length $F$ = 10 cm.

Figure 3 shows deviations of CC density from the regular background for a structure induced at $\lambda_0$ = 3100 nm (solid curve). It can be seen that the amplitude of CC density oscillations is maximum in the range of highest luminescence intensity (and, correspondingly, the strongest light field in the LB). To measure the period of CC density oscillations along the structure axis, they were automatically compared with the corresponding sinusoid (dashed curve). The result of this procedure (see Fig. 3) demonstrates strict periodicity of CC density oscillations along the filament practically in the entire range of existence of a LB by an example of the structure induced at $\lambda_0$ = 3100 nm and $F$ = 10 cm (the pulse propagated from the left to the right).

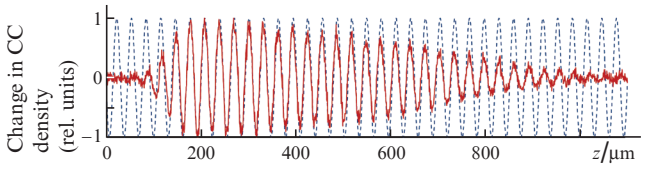


**Figure 3.** Determination of the period of CC density oscillations by an example of a structure induced by radiation with $\lambda_0 = 3100$ nm (focusing by a lens with $F = 10$ cm; the pulse propagates from the left to the right). The solid oscillating curve shows rapidly changing deviations of the CC density from a regular dependence (see Fig. 2). The dashed sinusoid demonstrates periodicity of changes in the CC density along the filament.

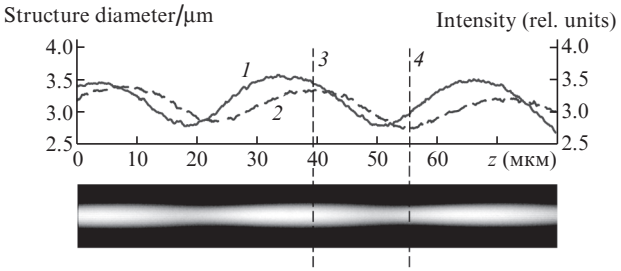


**Figure 4.** Continuous-tone image of a luminescence structure induced in LiF by a single 100-fs laser pulse at $\lambda_0 = 3100$ nm (bottom) and the dependences of the (*1*) axial luminescence intensity and (*2*) the structure diameter at half maximum on the longitudinal coordinate $z$, found based on this image. Curve (*1*) is normalised so as to provide visual alignment with curve (*2*). Vertical lines (*3*) and (*4*) indicate the points on the axis that correspond to the maximum and minimum diameters. The laser pulse propagates from the left to the right.

The period was measured on samples from 25 luminescence structures for each femtosecond laser wavelength and two values of the lens focal length. The induced structure periods were 36.5 ± 0.5, 31.2 ± 0.1 and 29.0 ± 0.1 μm when focusing by a lens with $F = 10$ cm at $\lambda_0 = 2600$, 3100 and 3350 nm, respectively, and 36.2 ± 0.5 and 31.0 ± 0.2 μm when focusing by a lens with $F = 15$ cm at $\lambda_0 = 2600$ and 3100 nm, respectively. The results of this analysis show that the period of induced structures increases with decreasing radiation wavelength and is independent of the lens focal length within the experimental error. The measurements of the period of the structures induced at $\lambda_0 = 3100$ nm and pulse energy varied in range of 9–15.6 μJ showed that the period does not change within an error of 3%. Thus, the period of CC density oscillations in the induced structures is a function of the excitation radiation wavelength and barely depends on the external focusing conditions and pulse energy. This finding confirms that the CC structures are induced in a filament by LBs, which are stable light field structures [21, 22].

The modulation depth of the longitudinal profiles of induced luminescence structures decreases with decreasing femtosecond radiation wavelength (Fig. 2). In the brightest parts of the structures, induced at $\lambda_0 = 2600$, 3100 and 3350 nm, the measured values of the luminescence intensity modulation depth, $(I_{max} - I_{min})/(I_{max} + I_{min})$, turned out to be about 5, 20 and 30%, respectively.

### 4.2. Peak CC density and diameter of induced structures

The induced structures were thoroughly studied using a PicoQuant MicroTime 200 confocal laser luminescence microscope with a 20× objective and radiation at $\lambda = 470$ nm for CC excitation. This tool made it possible to record images of induced structures with a resolution of 6.4 pixels $m^{-1}$ on a 80-μm scale (the resolution was limited by the working range of the piezoelectric scanner of the confocal microscope). Figure 4 shows an image of a luminescence structure induced in a filament at $\lambda_0 = 3100$ nm. Dependences of the CC density on the structure axis and its diameter (determined at half maximum) on the longitudinal coordinate were obtained by processing the transverse profiles of images (Fig. 4). It can be seen that the structure diameter oscillates along the axis; these oscillations are phase-shifted with respect to the CC density oscillations on the axis. A similar phase shift of the diameter and axial density oscillations was found in the images of the structures induced in a filament by beams with $\lambda_0 = 2600$ and 3350 nm.

Figure 5 shows transverse profiles of CC density ($\lambda_0 = 3100$ nm), measured in the cross sections with maximum [Fig. 4, line (*3*)] and minimum [Fig. 4, line (*4*)] diameters. The standard deviations of the profile width, obtained by averaging over five measurements, did not exceed 0.5%. The average diameters of the structures induced at $\lambda_0 = 2600$, 3100 and 3350 nm are, respectively, about 1.9, 3.0 and 3.2 μm; these values are close to the radiation wavelengths.

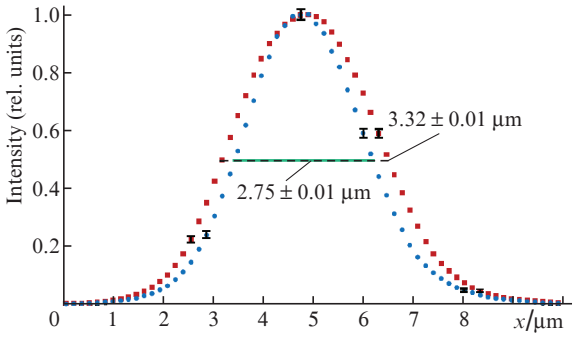


**Figure 5.** Normalised profiles for the luminescence CC structure induced by femtosecond radiation with $\lambda_0 = 3100$ nm, which were measured in the cross sections with the maximum and minimum diameters [see vertical lines (*3*) and (*4*) in Fig. 4]. The horizontal lines indicate the FWHM values for the profiles.

### 4.3. Influence of laser radiation wavelength on the induced-CC density

An analysis shows that the CC density in the structures induced at $\lambda_0 = 3100$ nm reaches larger values than in the structures induced at $\lambda_0 = 2600$ and 3350 nm. Figure 6 shows dependences of the axial luminescence intensity on the longitudinal coordinate, obtained at equal intensities but different wavelengths $\lambda_0$ of the excitation beam. Here, a region with the highest CC density was chosen in each structure. It can be seen that the highest CC density is obtained in the structure recorded at $\lambda_0 = 3100$ nm. This may be caused by direct generation of excitons during laser beam absorption in the medium. The efficiency of the direct excitonic channel of CC generation in alkali halide crystals is known to be comparable with that of the electron–hole channel [35]. We suggest that, in the case of multiphoton absorption of IR radiation, a reso-

nance occurs when the sum of the energies of an integer number $K$ of IR photons coincides with energy $E_{ex}$ of the exciton absorption band:

$$K\frac{hc}{\lambda_0} = E_{ex}, \quad (1)$$

where $h$ is Planck's constant and $c$ is the speed of light. Then, the concentration of generated excitons and, correspondingly, the CC density should periodically change with an increase in the photon energy. According to [36], the peak energy in the exciton absorption band, $E_{ex}$, is 12.8 eV, and the bandwidth is 0.25 eV. Radiation wavelengths $\lambda_0 = 2600$, 3100 and 3350 nm correspond to numbers of photons $K = 25.8$, 32.0 and 33.6, respectively. The deviation of the number of photons, $\Delta K$, with allowance for the exciton band and pulse spectrum widths, is $\pm 0.5$. For $\lambda_0 = 3100$ nm, $K$ is most close to an integer. Therefore, the radiation at this wavelength is closer to the resonance (1) than at wavelengths $\lambda_0 = 2600$ and 3350 nm.

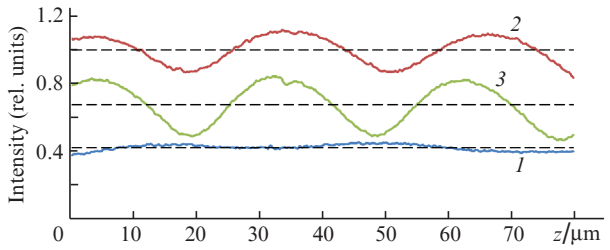


**Figure 6.** CC luminescence intensity on the structure axis, obtained at equal luminescence excitation intensities in the structures induced by femtosecond radiation with $\lambda_0 = (1)$ 2600, (2) 3100, and (3) 3350 nm. The dashed lines show the average intensity values.

### 4.4. Luminescence spectra of induced structures

Using a PicoQuant MicroTime 200 confocal microscope and an Ocean Optics QE65000 optical spectrometer, we recorded luminescence spectra of the induced structures in LiF. Figure 7 shows the luminescence spectrum of the structure induced at $\lambda_0 = 3100$ nm. Photoexcitation was performed by a laser with a sufficiently short wavelength ($\lambda = 405$ nm), which lies beyond the CC luminescence range. The spectrum contains two overlapping luminescence bands of CCs: one centred at $\lambda \approx 550$ nm for $F_3^+$ CCs and the other centred at $\lambda \approx 650$ nm for $F_2$ CCs.

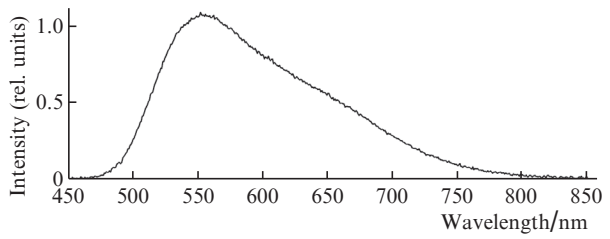


**Figure 7.** Luminescence spectrum (excitation at $\lambda = 405$ nm) of $F_3^+$ and $F_2$ colour centres in a structure induced by LB in LiF.

## 5. Numerical simulation

Numerical simulation reveals the scenario of the formation of the LB temporal structure, which leads to the observed modulation of the CC density. The formation and propagation of an LB in a medium was simulated using the equation for slowly varying complex field amplitude $A(r,z,t)$ with minimum approximation [37, 38], which is valid for wave packets with a width comparable with the optical oscillation period. The problem under consideration [22] was formalised taking into account the wave packet diffraction and dispersion, Kerr self-focusing, photoionisation and avalanche ionisation of the medium, defocusing and absorption of light in the induced plasma, and the pulse self-steepening. The material dispersion of LiF was calculated from the Sellmeier formula, and the photoionisation rate was determined using the Keldysh formalism [39]. The initial condition in the simulation corresponded to a pulse with a Gaussian temporal and spatial intensity distribution, the parameters of which were consistent with the experimental ones: the pulse FWHM was 100 fs and the pulse energy was 10.5, 15.5 and 18.0 μJ at $\lambda_0 = 2600$, 3100 and 3350 nm, respectively; this set corresponds to a peak power of about $1.5P_{cr}$, where $P_{cr}$ is the critical power for self-focusing in LiF.

The calculated distributions of light field intensity $I(r,\tau) \propto |A(r,\tau)|^2$ at $\lambda_0 = 3100$ nm and distances $z = 7.26$ and 7.59 mm from the input of the medium are shown in Fig. 8 in the local frame of reference for a pulse with a coordinate $\tau = t - z/v_g$, where $v_g$ is the pulse group velocity. A logarithmic colour scale was used to expand the range of reproducible intensities up to four orders of magnitude. The peak pulse intensity begins to grow rapidly at a distance of $z = 7.26$ mm (Fig. 8a); this rise corresponds to the LB formation onset. The peak pulse intensity becomes as high as $\sim 2 \times 10^{14}$ W cm$^{-2}$ at a distance of $z = 7.56$ mm (i.e., exceeds initial intensity $I_0$ by a factor of 150); this value is sufficient to implement multiphoton and avalanche ionisation and generate excitons [34] in a medium. In the case of strong anomalous GVD, the light field intensity increases due to the simultaneous spatial self-focusing and temporal self-compression of the pulse, which leads to the formation of an extremely compressed LB [21, 22] (Fig. 8b). The LB intensity FWHM becomes approximately 10 fs, which is about 10% of the initial pulse width. The thus formed LB is a stable wave packet, which contains several

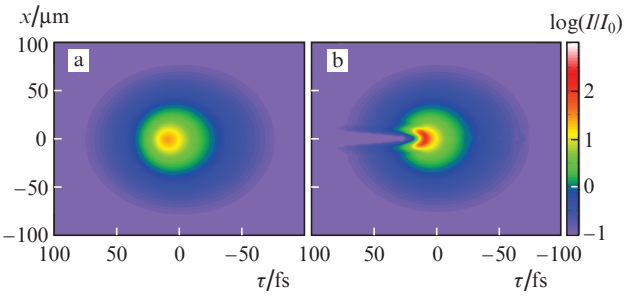


**Figure 8.** (Colour online) Spatial and temporal distributions of intensity $I$ in an LB formed from a 100-fs pulse with energy of 15.5 μJ at $\lambda_0 = 3100$ nm: (a) LB formation onset at $z = 7.26$ mm (peak intensity $3 \times 10^{13}$ W cm$^{-2}$, FWHM = 25 fs) and (b) the end of LB formation at $z = 7.56$ mm ($2 \times 10^{14}$ W cm$^{-2}$, 10 fs).

light field oscillations and propagates with a group velocity in a medium at a distance of about 1 mm.

The expression for the light-wave electric field strength $E(r,z,\tau)$ in the LB wave packet can be written as [37, 40]

$$E(r,z,\tau) = \frac{1}{2}A(r,z,\tau) \times \exp\left[i\omega_0\tau + iz\omega_0\left(\frac{1}{v_g} - \frac{1}{v_{ph}}\right)\right] + \text{c.c.}, \quad (2)$$

where $A(r,z,\tau) = |A(r,z,\tau)|\exp[i\xi(r,z,\tau)]$ is the calculated pulse complex envelope, $\omega_0 = 2\pi c/\lambda_0$ is the pulse carrier frequency, and $v_{ph} = c/n(\lambda_0)$ is the phase velocity. This equation describes the light field evolution in the wave packet with a change in envelope amplitude $|A(r,z,\tau)|$, envelope phase $\xi(r,z,\tau)$ and phase $\varphi(z) = z\omega_0(1/v_g - 1/v_{ph})$. Envelope phase $\xi(r,z,\tau)$ determines the spatial and temporal distribution of the phase shift of oscillations of the electric field $E(r,z,\tau)$ in the wave packet, which is caused by nonlinear optical conversion of light, whereas phase $\varphi(z)$ determines the time shift of light field oscillations with respect to the envelope peak; this shift is due to the difference between group velocity $v_g$ of the wave packet in the medium and phase velocity $v_{ph}$ at frequency $\omega_0$ in the dispersive medium. Note that, according to [1, 3, 4], a supercontinuum is generated under filamentation due to the self-phase modulation of the light field, at which the broadening of the frequency spectrum of the pulse is related to the temporal gradient of envelope phase $\xi(r,z,\tau)$, whereas the angular spectrum broadening is related to spatial gradient $\xi(r,z,\tau)$.

Figure 9a shows the light-wave electric field strength $E(r = 0,\tau)$ on the wave packet axis at a distance of $z$ = 7.26 mm, which corresponds to the initial stage of LB formation (see Fig. 8a). The pulse envelope contains several light wave cycles, and the peak electric field amplitude increases by a factor of about 5. At $z \approx 7.56$ mm, the pulse is extremely compressed, and a wave packet containing one optical oscillation is formed (Figs 9b–9d). Because of the difference in the phase and group velocities, $\Delta v = v_{ph} - v_g$, the light wave moves more rapidly than the wave packet envelope. It can be seen that, at $z_1$ = 7.559 mm (Fig. 9b), the maximum of the LB wave packet envelope coincides with the maximum of the light-wave amplitude, whereas at $z_2$ = 7.579 mm (Fig. 9c) the light wave shifts by a quarter of period and the resulting peak amplitude of the light field strength in the LB decreases by more than 20%. At $z_3$ = 7.596 mm (Fig. 9d), the maximum of the LB wave packet envelope coincides with the minimum of the light-wave amplitude, and the electric field strength amplitude becomes maximum again. Thus, when an LB propagates as a wave packet containing one light-wave period, the field amplitude periodically changes because of the difference in the group and phase velocities. These oscillations of the electric field peak amplitude occur in the entire range of LB existence.

The corresponding continuous-tone images of the distribution of light field strength $E(x, y = 0,\tau)$ in the wave packet cross section are shown in Figs 9e–9h. It can be seen that the light field wavefront is bent in the paraxial region of the newly formed LB; this bending is determined by envelope phase $\xi(r,z,\tau)$. The wavefront curvature for the first and central field oscillations in the LB is negative (which corresponds to positive Kerr nonlinearity of the medium) and positive for the field oscillations on the LB tail because of the defocusing in the self-induced laser plasma.

The LB diameter at an amplitude level of 80% of maximum is about 5 μm; this value is consistent with the transverse size of the experimentally observed CC structures (Fig. 4). A comparison of the images in Figs 9f–9h shows that the LB transverse size, as well as the maximum light field amplitude on the bullet axis, change periodically during LB propagation.

At $\lambda_0$ = 3100 nm, the band gap between the state of tightly bound exciton and the valence band (12.8 eV [36]) corresponds to the total energy of 32 laser photons. Therefore, a relatively small variation in the light field causes significant oscillations of CC density. These regular changes of the light

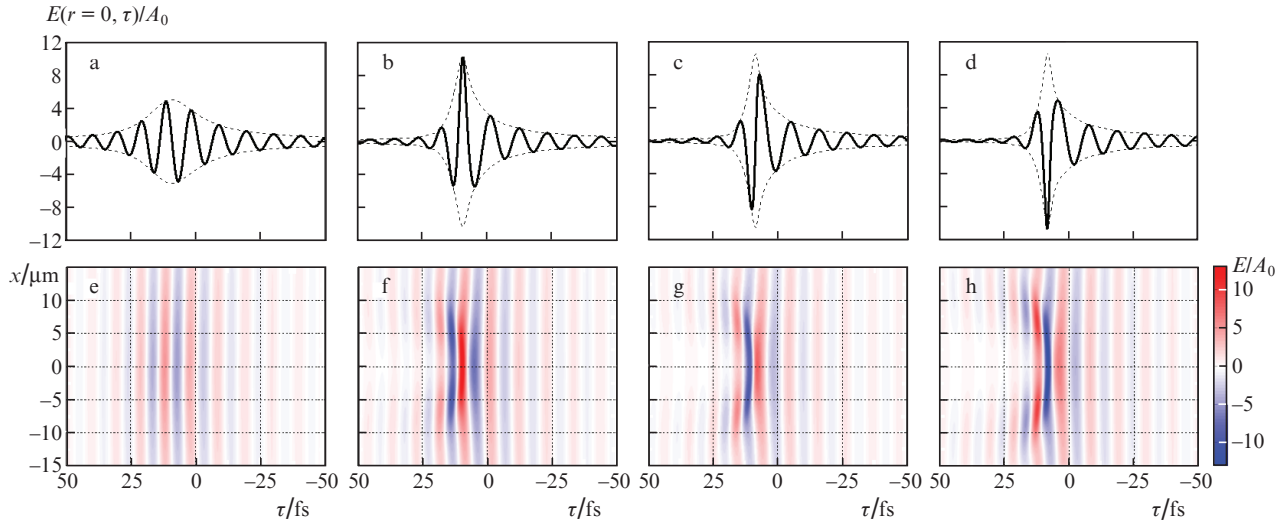


**Figure 9.** (Colour online) (a–d) Light field profiles on the LB axis and (e–h) continuous-tone images of the distribution of light field strength $E(x, y = 0,\tau)$ at the following distances from the input of the medium: (a, e) $z_0$ = 7.26 mm (initial stage of LB formation), (b, f) $z_1$ = 7.559 mm (the maximum of the LB wave packet envelope coincides with the maximum light-wave amplitude), (c, g) $z_2$ = 7.579 mm (the maximum of the LB wave packet envelope coincides with zero field in the light wave) and (d, h) $z_3$ = 7.596 mm (the maximum of the LB wave packet envelope coincides with the minimum of the light-wave amplitude); $A_0 = |A(0,0,0)|$.

field amplitude in LB, caused by the changes in phase $\varphi(z)$ during LB propagation in a medium, lead to the formation of a periodic CC structure under filamentation in the mid-IR range. The phase $\varphi(z)$ affects the nonlinear optical interaction between a laser pulse containing one field oscillation period and a medium with a characteristic time comparable with the optical oscillation period [40]. According to the numerical simulation data, period $\Delta z = \overline{z_3 - z_1}$ of the peak light field amplitude in the LB is 37.0 ± 0.5 μm at $\lambda_0$ = 3100 nm; at $\lambda_0$ = 3350 nm it decreases to 34.0 ± 0.5 μm, while at $\lambda_0$ = 2600 nm it rises to 42 ± 1 μm. The change in the obtained values of period $\Delta z$ with variation in wavelength corresponds to that observed in the experiment (see Subsection 4.1). The quantitative difference between the calculated and measured periods is related to possible deviation of the parameters of the medium used in the simulation from real ones.

A simple analytical estimate of the period of the light field peak amplitude in the LB can be found from the condition $\varphi(\Delta z^*) = \pi$, which neglects the influence of nonlinearity on the wave packet group velocity and phase modulation:

$$\Delta z^* = \frac{\lambda_0}{2n(\lambda_0)\Delta v} v_g. \quad (3)$$

At $\lambda_0$ = 3100 nm, formula (3) yields $\Delta z^*$ = 35 μm, which is in good agreement with the value found by numerical simulation. At $\lambda_0$ = 2600 and 3350 nm, we have $\Delta z^*$ = 42.6 and 32.4 μm, respectively; these values coincide with the experimentally found periods of the filament-induced CC structures in LiF.

The origin of the above-considered periodic structures in an isotropic LiF crystal differs from the nature of the structures observed previously in other media. The intensity oscillations along a filament in birefringent media are due to the periodic change in the pulse polarisation and the difference in the multiphoton absorption cross sections for linear and circular polarisations [41]. In this case, the period of intensity oscillations along the filament increases with an increase in the laser wavelength, in contrast to the structures induced in isotropic LiF. In the filamentation regime similar to the waveguide propagation under normal GVD conditions, which was studied numerically for a condensed medium [42] and for air [43], the period of the refocusing-induced intensity oscillations along the filament decreases (in comparison with the critical power for self-focusing) with a decrease in the laser pulse power. In a quasi-periodic sequence of LBs formed under filamentation in a medium with anomalous GVD, the gap between neighbouring bullets is not strictly periodic; moreover, its value exceeds greatly the CC density oscillation period in the structure induced in LiF under filamentation in the mid-IR range. The physical reason of the found periodic modulation of the CC density in LiF is the cyclic light field conversion in the LB propagating in LiF, which is caused by the change in the phase shift for the carrier wave and pulse envelope (due to the difference in the LB group and phase velocities).

## 6. Conclusions

The periodic changes in the CC density in a structure induced in an isotropic LiF crystal under filamentation of a mid-IR beam are caused by regular changes in the light field amplitude in the LB with a width of 1.5 periods, which are due to the difference between the LB envelope group velocity and the light-wave phase velocity. The periodic CC structures with a diameter close to the light wavelength are formed by an LB in the entire range of its existence (about 1 mm long). The period of changes in the CC density and diameter of induced structures is about 30 μm. The induced structure period is independent of the external focusing conditions and pulse energy, which confirms the stability of the LB, which is a result of the self-organisation of intense light field at its nonlinear optical interaction with a medium under anomalous GVD conditions. The study of the CC structures recorded in LiF under filamentation at different wavelengths revealed that the period of the CC density oscillations in the induced structures decreases with an increase in wavelength, whereas their amplitude increases. The highest CC density is obtained under filamentation at a wavelength of 3100 nm, which is due to the enhanced contribution of direct CC generation under absorption of an integer number of photons by the exciton band.

A numerical analysis of the light field evolution in an LB with a width of 1.5 optical periods revealed that a periodic change in the light-wave field strength amplitude during LB propagation leads to modulation of the CC density in LiF. The numerical simulation data are in agreement with the experimental results. The generation of stable luminescence CCs in an isotropic LiF crystal, which are characterised by high thermal and optical stability, makes it possible to investigate the spatial and temporal evolution of the LBs formed under filamentation of femtosecond mid-IR laser beams.

***Acknowledgements.*** We are grateful to T. Glushkova for measuring the optical parameters of LiF samples.

The work was supported by the Russian Foundation for Basic Research (Grant Nos) 14-22-02025-ofi_m and 15-32-50193-mol_nr) and the RF President's Grants Council (Support to Leading Scientific Schools Programme, Grant No. NSh-9695.2016.2).

## References

1. Chin S.L., Hosseini S.A., Liu W., Luo Q., Theberge F., Akozbek N., Becker A., Kandidov V., Kosareva O., Schroeder H. *Can. J. Phys*., **83**, 863 (2005).
2. Couairon A., Mysyrowicz A. *Phys. Rep*., **441**, 47 (2007).
3. Kandidov V.P., Shlenov S.A., Kosareva O.G. *Kvantovaya Elektron*., **39**, 205 (2009) [*Quantum Electron*., **39**, 205 (2009)].
4. Chin S.L. *Femtosecond Laser Filamentation* (New York: Springer, 2009).
5. Chekalin S.V., Kandidov V.P. *Usp. Fiz. Nauk*, **183** (2), 133 (2013).
6. Kasparian J., Wolf J.-P. *Opt. Express*, **16**, 466 (2008).
7. Chin S.L., Xu H.L., Luo Q., Théberge F., Liu W., Daigle J.-F., Kamali Y., Simard P.T., Bernhardt J., Hosseini S.A., Sharifi M., Méjean G., Azarm A., Marceau C., Kosareva O.G., Kandidov V.P., Aközbek N., Becker A., Roy G., Mathieu P., Simard P.T., Châteauneuf M., Dubois J. *Appl. Phys. B: Lasers Opt*., **95**, 1 (2009).
8. Valuev V.V., Dormidonov A.E., Kandidov V.P., Shlenov S.A., Kornienko V.N., Cherepenin V.A. *Radiotekh. Elektron*., **55** (2), 222 (2010).
9. Davis K.M., Miura K., Sugimoto N., Hirao K. *Opt. Lett*., **21**, 1729 (1996).
10. Gattass R.R., Cerami L.R., Mazur E. *Opt. Express*, **14**, 5279 (2006).
11. Silberberg Y. *Opt. Lett*., **15**, 1282 (1990).
12. Baranova N.B., Bykovskii N.E., Senatskii Yu.V., Chekalin S.V. *Tr. FIAN*, **103**, 84 (1978).
13. Smetanina E.O., Dormidonov A.E., Kandidov V.P. *Laser Phys*., **22**, 1189 (2012).

14. Smetanina E.O., Kompanets V.O., Dormidonov A.E., Chekalin S.V., Kandidov V.P. *Laser Phys. Lett*., **10**, 105401 (2013).
15. Chekalin S.V., Kompanets V.O., Smetanina E.O., Kandidov V.P. *Kvantovaya Elektron*., **43**, 326 (2013) [*Quantum Electron*., **43**, 326 (2013)].
16. Majus D., Tamošauskas G., Gražulevičiūtė I., Garejev N., Lotti A., Couairon A., Faccio D., Dubietis A. *Phys. Rev. Lett*., **112**, 193901 (2014).
17. Durand M., Jarnac A., Houard A., Liu Y., Grabielle S., Forget N., Durécu A., Couairon A., Mysyrowicz A. *Phys. Rev. Lett*., **110**, 115003 (2013).
18. Berge L., Skupin S. *Phys. Rev. E*, **71**, 065601 (2005).
19. Zaloznaya E.D., Dormidonov A.E. *Trudy VI Vseros. molodezhnoi konf. po fundamental'nym i innovatsionnym voprosam sovremennoi fiziki* (Proc. VI All-Russia Conf. of Young Scientists on Fundamental and Innovation Problems of Modern Physics) (Moscow: FIAN, 2015) p. 33.
20. Smetanina E.O., Kompanets V.O., Chekalin S.V., Dormidonov A.E., Kandidov V.P. *Book of Abstracts 4th Int. Symp. on Filamentation* (Tucson, Arizona, USA, 2012) p.129.
21. Chekalin S.V., Kompanets V.O., Dokukina A.E., Dormidonov A.E., Smetanina E.O., Kandidov V.P. *Kvantovaya Elektron*., **45**, 401 (2015) [*Quantum Electron*., **45**, 401 (2015)].
22. Chekalin S.V., Dokukina A.E., Dormidonov A.E., Kompanets V.O., Smetanina E.O., Kandidov V.P. *J. Phys. B: At. Mol. Opt. Phys*., **48**, 094008 (2015).
23. Krausz F., Ivanov M. *Rev. Mod. Phys*., **81**, 163 (2009).
24. Gražulevičiūtė I., Šuminas R., Tamošauskas G., Couairon A., Dubietis A. *Opt. Lett*., **40**, 3719 (2015).
25. Martynovich E.F., Kuznetsov A.V., Kirpichnikov A.V., Pestryakov E.V., Bagayev S.N. *Kvantovaya Elektron*., **43**, 463 (2013) [*Quantum Electron*., **43**, 463 (2013)].
26. Darginavičius J., Majus D., Jukna V., Garejev N., Valiulis G., Couairon A., Dubietis A. *Opt. Express*, **21**, 25210 (2013).
27. Dharmadhikari J.A., Deshpande R.A., Nath A., Dota K., Mathur D., Dharmadhikari A.K. *Appl. Phys. B*, **117**, 471 (2014).
28. Alisauskas S., Kartashov D.V., Pugzlys A., Faccio D., Zheltikov A.M., Voronin A., Baltuska A. *Techn. Dig. CLEO'2013* (San Jose, USA, 2013) QW1E.6.
29. Dormidonov A., Kompanets V., Chekalin S., Kandidov V. *Opt. Express*, **23**, 29202 (2015).
30. Baldacchini G. *J. Lumin*., **100**, 333 (2002).
31. Kurobori T., Kawamura K., Hirano M., Hosono H. *J. Phys.: Condens. Matter*., **15**, L399 (2003).
32. Stuart B.C., Feit M.D., Rubenchik A.M., Shore B.W., Perry M.D. *J. Opt. Soc. Am. B*, **13**, 459 (1996).
33. Kaiser A., Rethfeld B., Vicanek M., Simon G. *Phys. Rev. B*, **61**, 11437 (2000).
34. Mao S.S., Quéré F., Guizard S., Mao X., Russo R.E., Petite G., Martin P. *Appl. Phys. A*, **79**, 1695 (2004).
35. Lushchik Ch.B., Lushchik A.Ch. *Raspad elektronnykh vozbuzhdenii s obrazovaniem defektov v tverdykh telakh* (Decay of Electronic Excitations with Formation of Defects in Solids) (Moscow: Nauka, 1989).
36. Rohlfing M., Louie S.G. *Phys. Rev. Lett*., **81**, 2312 (1998).
37. Brabec T., Krausz F. *Phys. Rev. Lett*., **78**, 3282 (1997).
38. Couairon A., Brambilla E., Corti T., Majus D., de J. Ramírez-Góngora O., Kolesik M. *Eur. Phys. J. Spec. Top*., **199**, 5 (2011).
39. Keldysh L.V. *Zh. Eksp. Teor. Fiz*., **47**, 1945 (1964).
40. Brabec T., Krausz F. *Rev. Mod. Phys*., **72**, 545 (2000).
41. Blonskyi I., Kadan V., Shynkarenko Y., Yarusevych O., Korenyuk P., Puzikov V., Grin' L. *Appl. Phys. B*, **120**, 705 (2015).
42. Henz S., Herrmann J. *Phys. Rev. A*, **59**, 2528 (1999).
43. Fedorov V.Y., Tverskoy O.V., Kandidov V.P. *Appl. Phys. B*, **99**, 299 (2010).